



Article

An Optical Sensor with Polyaniline-Gold Hybrid Nanostructures for Monitoring pH in Saliva

Chongdai Luo^{1,2}, Yangyang Wang¹, Xuemeng Li¹, Xueqin Jiang¹, Panpan Gao¹, Kang Sun¹, Jianhua Zhou^{1,*}, Zhiguang Zhang² and Qing Jiang^{1,2}

¹ Key Laboratory of Sensing Technology and Biomedical Instruments of Guangdong Province, School of Engineering, Sun Yat-sen University, Guangzhou 510275, China; luochongdai@163.com (C.L.); wang45yangyang@163.com (Y.W.); lixm67@mail.sysu.edu.cn (X.L.); jiangxueqin4@126.com (X.J.); panpan.g@outlook.com (P.G.); sunk5@mail.sysu.edu.cn (K.S.); jqing@mail.sysu.edu.cn (Q.J.)

² Department of Oral and Maxillofacial Surgery, Guanghua School of Stomatology, Hospital of Stomatology, Guangdong Provincial Key Laboratory of Stomatology, Sun Yat-sen University, Guangzhou 510055, China; drzhangzg@163.com

* Correspondence: zhoujh33@mail.sysu.edu.cn; Tel./Fax: +86-20-3938-7890

Academic Editors: Chen-Zhong Li and Thomas Nann

Received: 3 August 2016; Accepted: 16 February 2017; Published: 17 March 2017

Abstract: Saliva contains important personal physiological information that is related to some diseases, and it is a valuable source of biochemical information that can be collected rapidly, frequently, and without stress. In this article, we reported a new and simple localized surface plasmon resonance (LSPR) substrate composed of polyaniline (PANI)-gold hybrid nanostructures as an optical sensor for monitoring the pH of saliva samples. The overall appearance and topography of the substrates, the composition, and the wettability of the LSPR surfaces were characterized by optical and scanning electron microscope (SEM) images, infrared spectra, and contact angles measurement, respectively. The PANI-gold hybrid substrate readily responded to the pH. The response time was very short, which was 3.5 s when the pH switched from 2 to 7, and 4.5 s from 7 to 2. The changes of visible-near-infrared (NIR) spectra of this sensor upon varying pH in solution showed that—for the absorption at given wavelengths of 665 nm and 785 nm—the sensitivities were 0.0299 a.u./pH (a.u. = arbitrary unit) with a linear range of pH = 5–8 and 0.0234 a.u./pH with linear range of pH = 2–8, respectively. By using this new sensor, the pH of a real saliva sample was monitored and was consistent with the parallel measurements with a standard laboratory method. The results suggest that this novel LSPR sensor shows great potential in the field of mobile healthcare and home medical devices, and could also be modified by different sensitive materials to detect various molecules or ions in the future.

Keywords: optical sensor; hybrid nanostructures; localized surface plasmon resonance; pH; saliva

1. Introduction

Human body fluids such as saliva represent a typical medium, containing important personal physiological information that is related with some diseases [1–8]. Saliva is also a valuable source of biochemical information [9,10] that is accessible in a non-invasive fashion, because it can be collected rapidly, frequently, and without stress. Compared to sweat and urine, saliva is more readily available—especially for those patients suffering from conditions that inhibit sweat production or who are suffering from chronic renal failure. These advantages are especially important in the field of mobile healthcare and home medical devices. For example, real-time monitoring of pH in saliva would be beneficial for monitoring mouth conditions (e.g., dental and enamel erosion) [11,12]; the decrease of pH reduced the corrosion resistance of titanium alloys and decreased the stability of their passive film in [13]. Additionally, pH in saliva is an indicator for some diseases. The saliva

of gastroesophageal reflux patients shows a reduction in pH when compared to normal individuals without the disease [14–17]. Low saliva pH is related to the presence of mucosal stomatitis [18], indicating a low secretion of saliva as well [19]. In some cases, drug activity depends on the pH of saliva [4]; the saliva pH and ionic composition may also influence the bioactivity of lysozyme [19].

On monitoring the pH of saliva, electrochemical and optical biosensors are the most commonly used. Among electrochemical sensors [20], glass-membrane electrodes [21], metal/metal oxide solid electrode [22], ion-selective electrodes [23], and ion-sensitive field effect transistors [24] have been developed. For example, Zuliani et al. developed a potentiometric disposable sensor that can monitor pH in sublingual saliva samples, which shows great potential for the integration of the sensor into a suitable in-mouth wearable device [23]. However, electrochemical methods have some disadvantages, such as interferences of ions in solution, desiccation, and easy contamination of the electrode. Optical methods such as fluorescent method and chemiluminescent method [21,25] are based on the detection of light emitting from the samples under radiation or chemical reaction. Usually, the detection systems for fluorescent and chemiluminescent methods are complex because the emitting light should be triggered; in addition, the detection is susceptible to the interference of background light from the environment. In addition, the samples should be labeled with fluorescent dyes or coupled with luminescent reagents before the detection.

Compared to the fluorescent and chemiluminescent methods, localized surface plasmon resonance (LSPR)-based biosensors based on the color changes visualized by the naked eye or the changes of ultraviolet-visible (UV-vis) spectra measured on a simple instrument are more promising. The sensor is composed of noble metal (e.g., gold) nanostructures, and shows an LSPR peak within the UV-vis-NIR region, and is highly sensitive to the refractive index of the environment near sensor surface. It is more sensitive and reliable than disposable pH test paper, which is based on color changes. It also holds the advantages of being label-free, high throughput, low-cost mass fabrication, and easy integration with mobile medical devices, and is therefore of great interest for many scientists [26].

Noble metal nanostructures featuring high surface area, small dimensions, and unique physical properties have strong plasmonic responses, and are competent materials for LSPR biosensors [27]. Various metal nanostructures have been fabricated with controlled shape and size [28,29]. Modification of nanostructures with active dielectric materials enables the plasmonic responses of various molecules [30], and thus they hold the potential to be developed into large-scale arrays composed of miniaturized signal transducer elements for the rapid detection of biomolecules and ions in the field of mobile healthcare and clinical diagnostics [31]. However, the application of nanostructures as LSPR sensing elements for monitoring the concentration of molecules or ions in a mouth has rarely been reported. Herein, the preparation and characterization of a simple LSPR sensor based on polyaniline (PANI)-gold hybrid nanostructures for monitoring the pH in saliva samples is presented. The sensor composed of polyaniline-gold hybrid nanostructures was prepared on a glass substrate. The pH sensitivity, response rate, and selectivity to pH sensor were investigated by a UV-vis-NIR spectrometer. Additionally, the pH of a real saliva sample was monitored using this sensor, and the results were consistent with the parallel measurements taken with a standard laboratory method.

2. Results and Discussion

The overall appearance and topography of the substrate is shown in Figure 1. The color of gold nanoplates (GNPs)-glass substrates (left) was dusty blue. After the coating of PANI, the color of PANI-GNPs-glass substrates (right) turned to green (Figure 1A). Spherical and irregular-shaped nanostructures can be observed in the scanning electron microscope (SEM) image, along with GNPs with edge length around 90–100 nm, and were randomly distributed on the glass substrate with a very low possibility of interparticle coupling due to the relatively large distance between different particles (Figure 1B). The observable core/shell nanostructures in the SEM image of PANI-GNPs-glass indicated that the GNPs-glass substrates were successfully covered by a layer of polymer (PANI) (Figure 1C). The positive charge of cetyltrimethylammonium bromide (CTAB) on the surface of GNPs made it easy

for aniline packaged in sodium dodecyl sulfate (SDS) micelles to be absorbed and immobilized onto the surface of GNPs-glass. Here, the sensor of PANI-GNPs-glass was composed of two parts: the GNPs on glass (acting as the sensing substrate) and the coating layer of PANI (acting as the sensing layer). The GNPs attached on glass exhibited an LSPR absorption peak, which was sensitive to changes in the refractive index of near the GNPs surface. The PANI layer that was coated onto the GNPs surface could show variations in its conductivity by controlling its proton-doping level, resulting in a remarkable change in its refractive index. Because the proton-doping level was dependent on the concentration of H^+ (i.e., pH), the variations in pH could manipulate proton-doping level of PANI and vary the refractive index of PANI near GNPs surface, leading to the changes of the LSPR absorption peak.

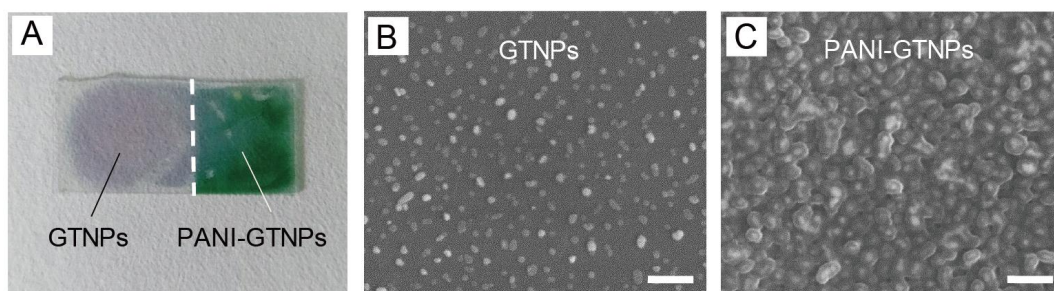


Figure 1. (A) Optical image of gold nanoplates (GNPs) and polyaniline (PANI)-GNPs on glass; scanning electron microscope (SEM) images of (B) GNPs; and (C) PANI-GNPs on glass. The scale bars in (B) and (C) are 400 nm.

An attenuated total reflection-Fourier transform infrared (ATR-FTIR) spectrometer was used to verify the composition of material on the surfaces of the as-prepared substrates (Figure 2). The ATR-FTIR spectra of PANI-glass, PANI-GNPs-glass, and GNPs-glass are shown in curves Figure 2a,b,c, respectively. In curve (a), the peaks of 1093 cm^{-1} , 1272 cm^{-1} , 1460 cm^{-1} , and 1572 cm^{-1} can be assigned to the N=Q=N stretching (Q is the quinonoid ring), C–N stretching vibration, C=C stretching of benzenoid ring, and C=C stretching of quinonoid ring, respectively [32]. In curve Figure 2b, the peaks of 1080 cm^{-1} and 1272 cm^{-1} can be ascribed to the N=Q=N stretching and C–N stretching vibration. It can be found that PANI and PANI-GNPs showed peaks revealing similar functional groups, implying that PANI was successfully coated onto the as-prepared GNPs-glass substrates.

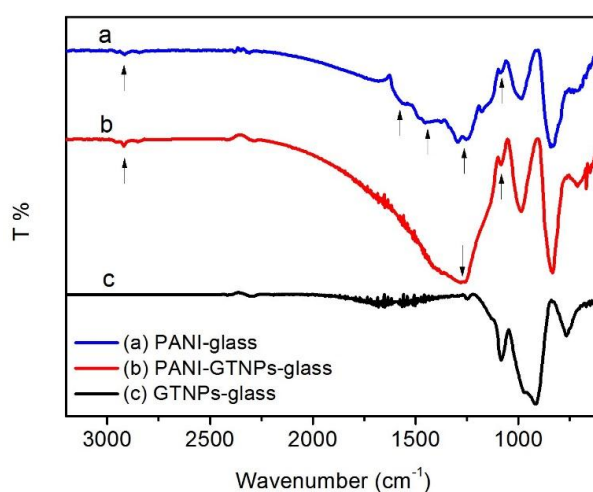


Figure 2. Attenuated total reflection-Fourier transform infrared (ATR-FTIR) spectra of PANI (curve a); PANI-GNPs (curve b); and GNPs (curve c) on glass. The three curves are offset for comparison. The peaks are indicated by arrows.

Surface water contact angle (CA) measurements were conducted to analyze the wettability of the sensor substrate surface. The CA of the glass surface was about 29° (Figure 3A), while the CA of the GNPs-glass substrate surface increased to 42° after the deposition of GNPs (Figure 3B). As shown in Figure 3C, the CA of the as-prepared PANI-GNPs-glass substrates was about 55° . Gradual increases of CA can be observed from bare glass to GNPs-glass, and then to PANI-GNPs-glass. It is clear to see that the surface of PANI-GNPs-glass was still very hydrophilic, which contributes to pH detection and monitoring in aqueous phase such as saliva.

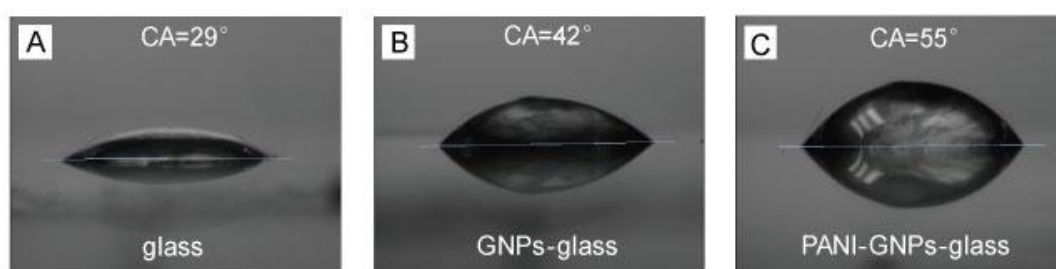


Figure 3. Surface water contact angle (CA) of (A) Glass; (B) GNPs-glass; and (C) PANI-GNPs-glass.

The comparison of visible-NIR spectra were observed before (Figure 4, curve a) and after (Figure 4, curve b) the coating of PANI on GNPs-glass substrates. The LSPR dipole peak of GNPs can be obviously seen in the near-infrared region in curve Figure 4a. After the coating of PANI, the PANI-GNPs-glass substrate was obtained. The spectrum of PANI-GNPs-glass substrates is shown in curve Figure 4b, with an increase of absorption around 625 nm, which is from PANI. As we can see from curve Figure 4b, there are two main peaks in the visible-NIR spectrum—one is in the visible light region (from PANI), and the other one is in NIR region (from GNPs). The peak in visible light region (assigned to PANI) can be affected by the pH of the bulk solution that the sensor substrates interfaced. The other one in the NIR region was mainly from the LSPR of GNPs, which was sensitive to the refractive index of PANI around the GNPs.

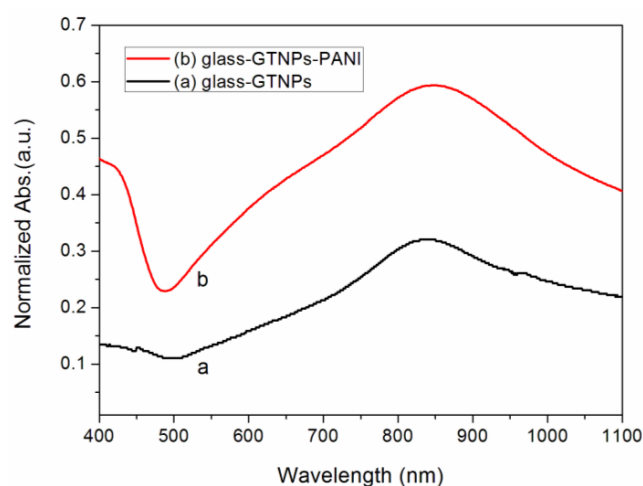


Figure 4. Visible-near-infrared (Visible-NIR) spectra of GNPs (curve a) and PANI-GNPs (curve b) on glass in water (pH = 6.5).

We conducted a quantitative analysis of PANI-GNPs-glass sensor substrates, including the visible-NIR spectra of the substrates in bulk solutions with different pH (pH = 2–8) (Figure 5). As shown in Figure 5A, the visible-NIR spectra of PANI-GNPs-glass substrates changed regularly with the pH of the bulk solutions. The peak in the NIR region became higher and had a small blue shift when the pH

of bulk solutions decreased. The peak in the visible light region became higher when the pH increased. The changes in spectra can be attributed to the response of PANI structure to pH and the LSPR changes of GNPs. These regular and detectable changes make pH detection by PANI-GNPs-glass substrates possible. As illustrated in Figure 5A, to make the sensor substrates more credible, absorption at 665 nm was measured along with 785 nm, which could be applied to double-wavelength calibration. All data reported in this paper was based on the absorption at one or two specific wavelengths. The absorption at 665 nm and 785 nm in bulk solutions with different pH is shown in Figure 5B,C, respectively. Figure 5D shows the linear ranges and the sensitivities of the sensor at these two wavelengths. The sensitivity of PANI-GNPs-glass sensor was found to be higher when the measurement was performed at a given wavelength of 665 nm, compared with that at 785 nm. As for the absorption at these two wavelengths (665 nm and 785 nm), the PANI-GNPs-glass substrate of the sensor showed corresponding sensitivities of 0.0299 a.u./pH in linear range pH = 5–8 and 0.0234 a.u./pH in linear range pH = 2–8, respectively. It is worth mentioning that the linear ranges of pH measurement of this PANI-GNPs-glass sensor can be changed by tuning the LSPR peaks of GNPs. Since the location of the LSPR peak of the GNPs can be affected by the sizes and inter-distances of GNPs on glass, the overlap between the LSPR peak of GNPs and visible-NIR absorption peak of PANI could be regulated to prepare a series of PANI-GNPs-glass substrates with different spectra. When the spectra of the substrates were different, the responsive behaviors of spectra to pH varied, and the linear ranges of pH measurement would be changed accordingly.

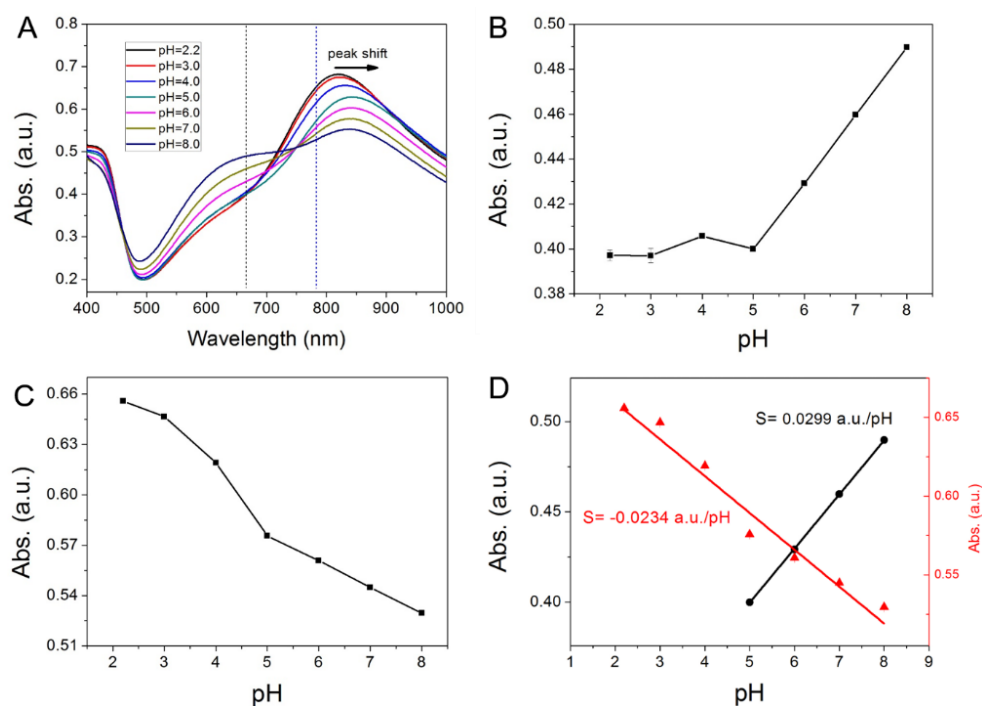


Figure 5. (A) Visible-NIR spectra of PANI-GNPs-glass in pH = 2.2, 3.0, 4.0, 5.0, 6.0, 7.0, 8.0 media; (B) The changes of absorbance at 665 nm in different pH media; (C) The changes of absorbance at 785 nm in different pH media; (D) Two pH linear ranges of this PANI-GNPs-glass biosensor based on absorbance at 665 nm (black) and absorbance at 785 nm (red).

The response behavior, response rate, and reversibility of the PANI-GNPs-glass sensor are presented in Figure 6. As shown in Figure 6A, the substrate was green in acidic bulk solution and then turned blue in alkali bulk solution. The response time of PANI-GNPs-glass at 785 nm from pH = 2 to pH = 7 (Figure 6B) and from pH = 7 to pH = 2 (Figure 6C) was 3.5 s and 4.5 s, respectively. This quick-acting response time makes PANI-GNPs-glass a promising sensor for pH monitoring, not only

one-time pH detection. Figure 6D shows the absorption at 785 nm of the PANI-GNPs-glass sensor in different pH environments (switching three cycles between pH = 2 and pH = 7). It can be observed that three absorption data points of pH = 2 were stable and also with pH = 7. This reversible switch of absorption at a given wavelength can be explained by the chemical structure of PANI. HCl reacts with PANI to give the proton-doped emeraldine form, which is a p-type semiconductor and has a larger electrical conductivity. Proton dedoping is realized by supplying NaOH to neutralize the acid and recover the undoped emeraldine form of PANI, which has a smaller conductivity. At the undoped and doped states of the PANI layer, the nanostructures show distinct spectra in the visible-NIR region, which lead to the change in absorption at a given wavelength [30]. This stability of absorption at 785 nm proved the good reversibility of PANI-GNPs-glass sensor, which makes PANI-GNPs-glass promising for pH monitoring.

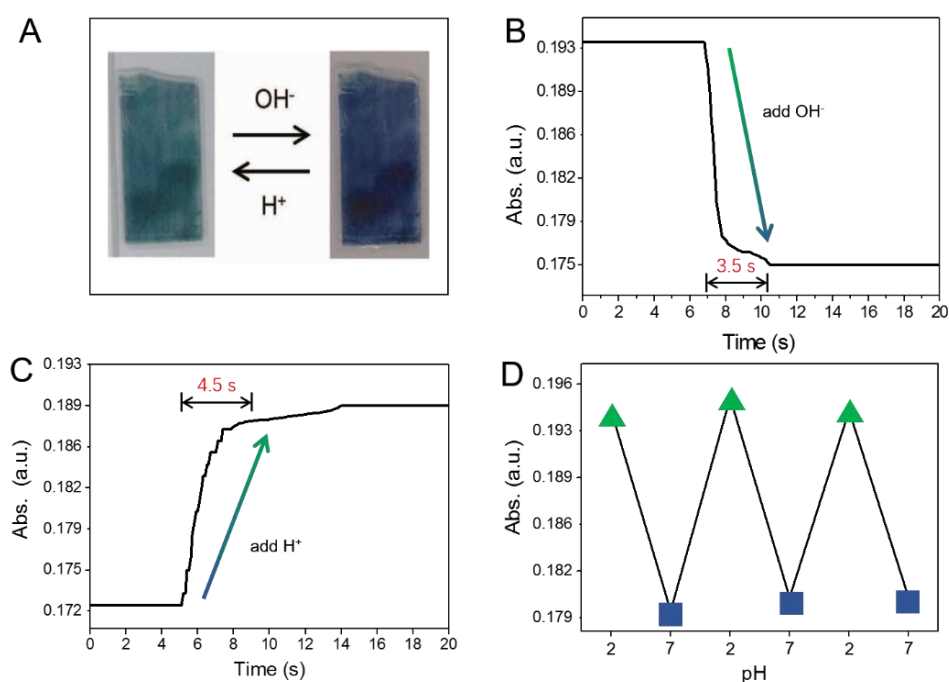


Figure 6. (A) Optical images of PANI-GNPs-glass, showing the color changes between acid (low pH) and alkaline (high pH) medium; (B) The response curve from acid medium (pH = 2) to alkaline medium (pH = 7) at 785 nm; (C) The response curve from alkaline medium (pH = 7) to acid medium (pH = 2) at 785 nm; (D) The absorbance changes of PANI-GNPs-glass biosensor at 785 nm upon switching between pH = 2 and 7 media (three cycles).

Figure 7 shows the response of PANI-GNPs-glass to some of the main components in saliva, including some electrolytes (e.g., K⁺, Ca²⁺, H⁺, HCO₃⁻, HPO₄²⁻), some small molecules (e.g., urea), and proteins. Proteins in saliva were represented by bovine serum albumin (BSA) in this experiment. All the electrolytes, molecules, and proteins were applied with the typical concentration in the saliva of a normal human being. The absorption at 785 nm of PANI-GNPs-glass was measured. The response of PANI-GNPs-glass sensor to H⁺ (pH = 2) was the highest among the main components. The responses of the sensor to K⁺ and Ca²⁺ were very low, and so was the protein representative BSA. However, the responses of the sensor to HCO₃⁻, HPO₄²⁻, and urea were high, and we found that urea was the main interference to pH measurement in this experiment. Further research on the principle of PANI-GNPs-glass responding to urea will be conducted in the future to eliminate the interference of urea.

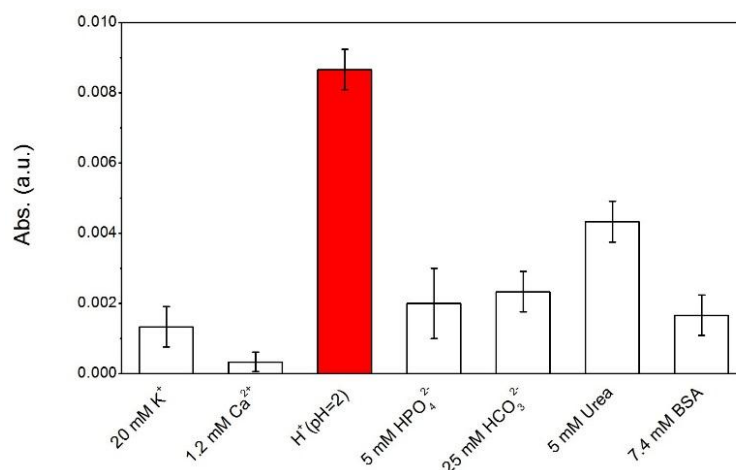


Figure 7. The responses of PANI-GNPs-glass to the main components in saliva, including some electrolytes, proteins, and small organic molecules at 785 nm. The concentrations of electrolytes and proteins that we used here were the typical level of the concentration of all the components in real saliva. *Abs* was used to represent the response of the sensor to a component in saliva ($Abs = |Abs_c - Abs_0|$, Abs_0 is the absorbance of the sensor in PBS (pH = 7.4); Abs_c is the absorbance of the sensor in PBS mixed with some main component in saliva). The error bars represent ± 1 standard deviation of the mean for three different measurements. PBS: phosphate buffer solution; BSA: bovine serum albumin.

In order to demonstrate the ability, sensitivity, and stability of the PANI-GNPs-glass substrate as a sensor to monitor the pH in real sample, the pH of a diluted saliva sample from a normal person was monitored (Figure 8). HCl solution (pH = 1) with a pre-calculated volume was added into the saliva sample to adjust the pH. We have recorded the trace of the absorbance with HCl solution (pH = 1) titration. The time-point of HCl solution (pH = 1) titrations were indicated with the arrows on the graph. While the pH changed from 6 to 5, 4, and then 3, the sensor showed a successive increase of absorbance. At each time-point of adding HCl solution, a sharp increase of absorbance was observed, followed by a constant increase until the absorbance reached a stable point. The response rate and stability of PANI-GNPs-glass biosensor to pH were excellent in real saliva sample monitoring, suggesting that PANI-GNPs-glass can be a promising sensor for saliva pH monitoring.

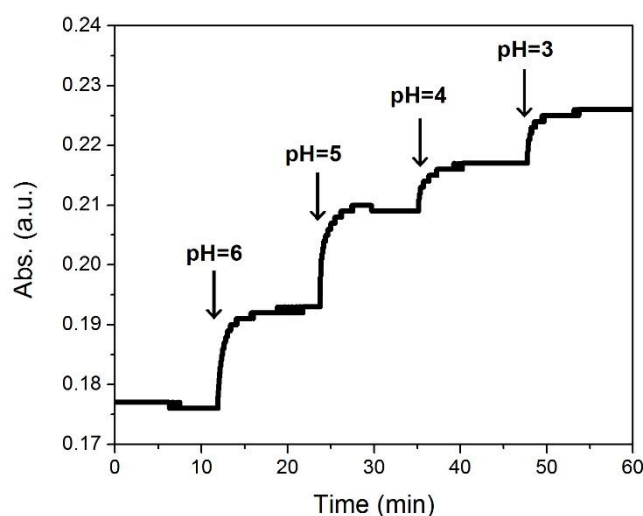


Figure 8. The real-time pH monitoring of a saliva sample (from a normal person) using a PANI-GNPs-glass biosensor at 785 nm. The time-point of HCl solution (pH = 1) titrations are indicated with arrows.

3. Experimental Section

3.1. Chemicals and Materials

Gold (III) chloride trihydrate ($\text{HAuCl}_4 \cdot 3\text{H}_2\text{O}$, >99.0%), sodium borohydride (NaBH_4 , 99%), L-ascorbic acid ($\text{C}_6\text{H}_8\text{O}_6$, >99%), potassium iodide (KI, 99%), aniline monomer (>99.9%), ammonium persulphate (APS, 99.99%) and sodium dodecyl sulfate (SDS, 97%) were purchased from Aladdin Chemical Co., Ltd. (Shanghai, China); cetyltrimethylammonium bromide (CTAB, 99%), trisodium citrate ($\text{C}_6\text{H}_5\text{O}_7\text{Na}_3 \cdot 2\text{H}_2\text{O}$, 99.00%), sodium hydroxide (NaOH , 97.00%), and sodium chloride (NaCl , 99.50%) were purchased from Damao Chemical Co., Ltd. (Tianjin, China). Deionized water was prepared by a Milli-Q Advantage A10 water system (Millipore, Billerica, MA, USA) with a resistivity of 18.2 $\text{M}\Omega \cdot \text{cm}$.

3.2. Synthesis of GNPs

The GNPs were prepared following a seed-mediated growth approach as previously described [33]. By this approach, the mixture was obtained with expected GNPs and byproducts, such as gold spherical nanoparticles and gold nanorods. The high-yield GNPs was separated by following a procedure modified from a previously reported method [34].

3.3. Preparation of GNPs-Glass Substrate

Before the deposition of GNPs, glass slides were successively immersed in aqua regia and piranha acid with extreme care. Then slides were rinsed thoroughly with deionized water, kept in ethanol under ultrasonication for 30 min, and then dried in oven at 80 °C for 0.5 h. GNPs solution containing ~2 μM CTAB were obtained by centrifuging the as-prepared suspension of GNPs containing 0.1 M CTAB solutions (10 mL), removing the supernatant, and redispersing the precipitated nanoplates into deionized water (10 mL) as previously reported [35]. This procedure was repeated twice. At each step, ~40–50 μL residual solution was left in the centrifuge tube; the concentration of CTAB was therefore estimated to ~2 μM in the final supernatant. Finally, the substrate coated with the GNPs (i.e., GNPs-glass substrate) was prepared by dripping the GNPs solution (containing ~2 μM CTAB) onto a glass slide and then dried.

3.4. Coating Polyaniline (PANI) onto GNPs-Glass Substrate

The coating of PANI onto the GNPs-glass substrate was performed as follows. A GNPs-glass substrate was dipped into a mixed solution containing aniline monomer (2.0 mM), SDS (40 mM), and APS (2 mM, pH 2.0) with volume ratio of 6:1:6 at room temperature for 6 h. The substrates were then rinsed with deionized water and dried at room temperature, and the GNPs-glass substrates coated with PANI (i.e., PANI-GNPs-glass) were obtained.

3.5. Measuring the pH Sensitivity of PANI-GNPs-Glass Substrate

The PANI-GNPs-glass substrate was fixed onto the wall of a transparent cuvette filled with solution. The substrate was perpendicular to the optical path of a UV-vis spectrometer, with the PANI-GNPs side toward the solution. The pH switching of solution between 2 and 7 was adjusted by adding HCl (pH = 1) or NaOH (pH = 13) solution into the solution. To adjust the pH of the real saliva sample, we diluted saliva five-fold by deionized water. HCl solution of 0.165 mL (pH = 5), 0.185 mL (pH = 4), 0.205 mL (pH = 3), 0.230 mL (pH = 2), 0.255 mL (pH = 1) were successively added into the 1.5 mL sample of saliva. At each point of pH, the spectrum of PANI-GNPs-glass substrate was recorded.

3.6. Characterization

The optical images of the substrates were taken by using a cell-phone camera (Sony, Tokyo, Japan). Scanning electron microscopy (SEM) images were taken with a scanning electron microscope

JEOL JSM-6330F (JEOL, Tokyo, Japan). Infrared (IR) spectra were recorded with the wavenumbers ranging from 600 to 4000 cm^{-1} on a Fourier transform infrared (FT-IR) spectrometer Bruker VERTEX 70 (Bruker Optics, Ettlingen, Germany) with an ATR accessory. The contact angle was measured by using a contact angle meter JC2000C1 (POWEREACH, Shanghai, China). The UV-vis spectra were obtained from a UV-vis-NIR spectrophotometer Inesa L3S (INESA, Shanghai, China).

4. Conclusions

We have fabricated an optical sensor composed of polyaniline–gold hybrid nanostructures, and applied it in monitoring the pH of saliva. Compared with previous techniques such as electrochemical sensors and ion-sensitive field effect transistors, the optical sensor holds the following advantages: (1) unlike the electrochemical method, the optical sensor is more stable to the interference of the electrolyte ions and the fluctuations of their concentration; (2) because the measurement wavelength (e.g., 785 nm) is located in the bio-window of tissue, the optical sensor is supposed to be more resistant to the biological adsorption such as the common protein/bacteria in the oral cavity. The sensor is able to measure the pH changes ranging from 2.0 to 8.0 by measuring the absorbance changes or peak shift of its UV-vis spectra (Figure S1). The sensor with excellent reversibility demonstrates a potential ability for real-time monitoring. Compared to other optical sensors, this kind of PANI-GNPs-glass optical sensor can achieve different linear ranges of pH measurement by tuning the interaction between the LSPR peak of GNPs and visible-NIR absorption peak of PANI. In addition, two main characteristic peaks in the visible-NIR spectra of the PANI-GNPs-glass substrate make this sensor possible to use double-wavelength calibration. Our results also show that this GNPs-based LSPR sensor could be modified by different sensitive materials to detect various molecules or ions in the field of rapid diagnosis, mobile healthcare, and environmental monitoring.

Supplementary Materials: The supplementary materials are available online at <http://www.mdpi.com/2079-4991/7/3/67/s1>.

Acknowledgments: This work was supported in part by the National Natural Science Foundation of China (No. 21405183), the special support plan for training high-level talents in Guangdong Province (No. 2014TQ01R695), and the Fundamental Research Funds for the Central Universities (No. 16lgjc62). The work was also supported in part by the Australia-China Joint Institute for Health Technology and Innovation.

Author Contributions: Chongdai Luo, Yangyang Wang and Xueqin Jiang did the experiments and prepared the manuscript; Xueming Li planned the experiments and revised the manuscript; Panpan Gao and Kang Sun advised the work and modified the manuscript; Jianhua Zhou designed the experiments and wrote the manuscript; Zhiguang Zhang and Qing Jiang provided valuable suggestions and edited the draft.

Conflicts of Interest: The authors declare no conflict of interest.

References

1. Papacosta, E.; Nassis, G.P. Saliva as a tool for monitoring steroid, peptide and immune markers in sport and exercise science. *J. Sci. Med. Sport* **2011**, *14*, 424–434. [[CrossRef](#)] [[PubMed](#)]
2. Ljungberg, G.; Ericson, T.; Ekblom, B.; Birkhed, D. Saliva and marathon running. *Scand. J. Med. Sci. Sports* **1997**, *7*, 214–219. [[CrossRef](#)] [[PubMed](#)]
3. Khaustova, S.A.; Shkurnikov, M.U.; Tonevitsky, A.G. Short highly intense exercise causes changes in salivary concentrations of hydrocortisone and secretory IgA. *Bull. Exp. Biol. Med.* **2010**, *149*, 635–639. [[CrossRef](#)] [[PubMed](#)]
4. Ghimenti, S.; Lomonaco, T.; Onor, M.; Murgia, L.; Paolicchi, A.; Fuoco, R.; Ruocco, L.; Pellegrini, G.; Trivella, M.G.; Francesco, F.D. Measurement of warfarin in the oral fluid of patients undergoing anticoagulant oral therapy. *PLoS ONE* **2011**, *6*, e28182. [[CrossRef](#)] [[PubMed](#)]
5. Herr, A.E.; Hatch, A.V.; Giannobile, W.V.; Throckmorton, D.J.; Tran, H.M.; Brennan, J.S.; Singh, A.K. Integrated microfluidic platform for oral diagnostics. *Ann. N. Y. Acad. Sci.* **2007**, *1098*, 362–374. [[CrossRef](#)] [[PubMed](#)]

6. Yang, C.Y.; Brooks, E.; Li, Y.; Denny, P.; Ho, C.M.; Qi, F.X.; Shi, W.Y.; Wolinsky, L.; Wu, B.; Wong, D.T.W. Detection of picomolar levels of interleukin-8 in human saliva by SPR. *Lab Chip* **2005**, *5*, 1017–1023. [[CrossRef](#)] [[PubMed](#)]
7. Yoda, K.; Shimazaki, K.; Ueda, Y. Analysis of glycolysis relevant compounds in saliva by microbiosensors. *Ann. N. Y. Acad. Sci.* **1998**, *864*, 600–604. [[CrossRef](#)] [[PubMed](#)]
8. Diamond, D. Peer reviewed: Internet-scale sensing. *Anal. Chem.* **2004**, *76*, A278–A286. [[CrossRef](#)]
9. Arakawa, T.; Kuroki, Y.; Nitta, H.; Chouhan, P.; Toma, K.; Sawada, S.; Takeuchi, S.; Sekita, T.; Akiyoshi, K.; Minakuchi, S.; et al. Mouthguard biosensor with telemetry system for monitoring of saliva glucose: A novel cavitas sensor. *Biosens. Bioelectron.* **2016**, *84*, 106–111. [[CrossRef](#)] [[PubMed](#)]
10. Du, Y.Q.; Zhang, W.J.; Wang, M.L. Sensing of salivary glucose using nano-structured biosensors. *Biosensors* **2016**, *6*, 10–24. [[CrossRef](#)] [[PubMed](#)]
11. Millward, A.; Shaw, L.; Harrington, E.; Smith, A.J. Continuous monitoring of salivary flow rate and pH at the surface of the dentition following consumption of acidic beverages. *Caries Res.* **1997**, *31*, 44–49. [[CrossRef](#)] [[PubMed](#)]
12. Batista, G.R.; Torres, C.R.G.; Sener, B.; Attin, T.; Wiegand, A. Artificial saliva formulations versus human saliva pretreatment in dental erosion experiments. *Caries Res.* **2016**, *50*, 78–86. [[CrossRef](#)] [[PubMed](#)]
13. Robin, A.; Meirelis, J.P. Influence of fluoride concentration and pH on corrosion behavior of Ti-6Al-4V and Ti-23Ta alloys in artificial saliva. *Mater. Corros.* **2007**, *58*, 173–180. [[CrossRef](#)]
14. Eckley, C.A.; Costa, H.O. Comparative study of salivary pH and volume in adults with chronic laryngopharyngitis by gastroesophageal reflux disease before and after treatment. *Braz. J. Otorhinolaryngol.* **2006**, *72*, 55–60. [[CrossRef](#)]
15. Bouchoucha, M.; Callais, F.; Renard, P.; Ekindjian, O.G.; Cugnenc, P.H.; Barbier, J.P. Relationship between acid neutralization capacity of saliva and gastro-oesophageal reflux. *Arch. Physiol. Biochem.* **1997**, *105*, 19–26. [[CrossRef](#)] [[PubMed](#)]
16. Lazarchik, D.A.; Filler, S.J. Effects of gastroesophageal reflux on the oral cavity. *Am. J. Med.* **1997**, *103*, S107–S113. [[CrossRef](#)]
17. Sujatha, S.; Jalihal, U.; Devi, Y.; Rakesh, N.; Chauhan, P.; Sharma, S. Oral pH in gastroesophageal reflux disease. *Indian J. Gastroenterol.* **2016**, *35*, 186–189. [[CrossRef](#)] [[PubMed](#)]
18. Martori, E.; Ayuso-Montero, R.; Martinez-Gomis, J.; Viñas, M.; Peraire, M. Risk factors for denture-related oral mucosal lesions in a geriatric population. *J. Prosthet. dent.* **2014**, *111*, 273–279. [[CrossRef](#)] [[PubMed](#)]
19. Dodds, M.W.J.; Johnson, D.A.; Yeh, C.K. Health benefits of saliva: A review. *J. Dent.* **2005**, *33*, 223–233. [[CrossRef](#)] [[PubMed](#)]
20. Zhang, L.; Zhang, Q.; Lu, X.B.; Li, J.H. Direct electrochemistry and electrocatalysis based on film of horseradish peroxidase intercalated into layered titanate nano-sheets. *Biosens. Bioelectron.* **2007**, *23*, 102–106. [[CrossRef](#)] [[PubMed](#)]
21. Imfeld, T.N. Identification of low caries risk dietary components. *Monogr. Oral Sci.* **1983**, *11*, 1–198. [[PubMed](#)]
22. Ayazi, S.; Lipham, J.C.; Hagen, J.A.; Tang, A.L.; Zehetner, J.; Leers, J.M.; Oezcelik, A.; Abate, E.; Banki, F.; DeMeester, S.R. A new technique for measurement of pharyngeal pH: Normal values and discriminating pH threshold. *J. Gastrointest. Surg.* **2009**, *13*, 1422–1429. [[CrossRef](#)] [[PubMed](#)]
23. Zuliani, C.; Matzeu, G.; Diamond, D. A potentiometric disposable sensor strip for measuring pH in saliva. *Electrochim. Acta* **2014**, *132*, 292–296. [[CrossRef](#)]
24. Visch, L.L.; Bergveld, P.; Lamprecht, W. pH measurements with an ion sensitive field effect transistor in the mouth of patients with xerostomia. *IEEE Trans. Biomed. Eng.* **1991**, *38*, 353–356. [[CrossRef](#)] [[PubMed](#)]
25. Tan, X.J.; Song, Z.H. Continuous, quantitative monitoring of roxithromycin in human saliva by flow injection chemiluminescence analysis. *Appl. Spectrosc.* **2013**, *67*, 54–58. [[CrossRef](#)] [[PubMed](#)]
26. Shen, Y.; Zhou, J.H.; Liu, T.R.; Tao, Y.T.; Jiang, R.B.; Liu, M.X.; Xiao, G.H.; Zhu, J.H.; Zhou, Z.K.; Wang, X.H.; et al. Plasmonic gold mushroom arrays with refractive index sensing figures of merit approaching the theoretical limit. *Nat. Commun.* **2013**, *4*, 2381–2389. [[CrossRef](#)] [[PubMed](#)]
27. Zhou, J.H.; Zeng, J.; Grant, J.; Wu, H.K.; Xia, Y.N. On-chip screening of experimental conditions for the synthesis of noble-metal nanostructures with different morphologies. *Small* **2011**, *7*, 3308–3316. [[CrossRef](#)] [[PubMed](#)]
28. Xia, X.H.; Zeng, J.; Zhang, Q.; Moran, C.H.; Xia, Y.N. Recent developments in shape-controlled synthesis of silver nanocrystals. *J. Phys. Chem. C* **2012**, *116*, 21647–21656. [[CrossRef](#)] [[PubMed](#)]

29. Joshi, G.K.; McClory, P.J.; Muhoberac, B.B.; Kumbhar, A.; Smith, K.A.; Sardar, R. Designing efficient localized surface plasmon resonance-based sensing platforms: Optimization of sensor response by controlling the edge length of gold nanoprisms. *J. Phys. Chem. C* **2012**, *116*, 20990–21000. [[CrossRef](#)]
30. Jiang, N.N.; Shao, L.; Wang, J.F. (Gold nanorod core)/(polyaniline shell) plasmonic switches with large plasmon shifts and modulation depths. *Adv. Mater.* **2014**, *26*, 3282–3289. [[CrossRef](#)] [[PubMed](#)]
31. Sreekanth, K.V.; Alapan, Y.; ElKabbash, M.; Ilker, E.; Hinczewski, M.; Gurkan, U.A.; De Luca, A.; Strangi, G. Extreme sensitivity biosensing platform based on hyperbolic metamaterials. *Nat. Mater.* **2016**, *15*, 621–628. [[CrossRef](#)] [[PubMed](#)]
32. Shen, J.L.; Yang, C.Y.; Li, X.W.; Wang, G.C. High-performance asymmetric supercapacitor based on nanoarchitected polyaniline/graphene/carbon nanotube and activated graphene electrodes. *ACS Appl. Mater. Interfaces* **2013**, *5*, 8467–8476. [[CrossRef](#)] [[PubMed](#)]
33. Jiang, X.Q.; Liu, R.M.; Tang, P.J.; Li, W.B.; Zhong, H.X.; Zhou, Z.K.; Zhou, J.H. Controllably tuning the near-infrared plasmonic modes of gold nanoplates for enhanced optical coherence imaging and photothermal therapy. *RSC Adv.* **2015**, *5*, 80709–80718. [[CrossRef](#)]
34. Liu, R.M.; Zhou, J.H.; Zhou, Z.K.; Jiang, X.Q.; Liu, J.M.; Liu, G.H.; Wang, X.H. On-demand shape and size purification of nanoparticle based on surface area. *Nanoscale* **2014**, *6*, 13145–13153. [[CrossRef](#)] [[PubMed](#)]
35. Shao, L.; Ruan, Q.F.; Jiang, R.B.; Wang, J.F. Macroscale colloidal noble metal nanocrystal arrays and their refractive index-based sensing characteristics. *Small* **2014**, *10*, 802–811. [[CrossRef](#)] [[PubMed](#)]



© 2017 by the authors. Licensee MDPI, Basel, Switzerland. This article is an open access article distributed under the terms and conditions of the Creative Commons Attribution (CC BY) license (<http://creativecommons.org/licenses/by/4.0/>).